

Article

Not peer-reviewed version

Linear and Nonlinear Optical Properties of Non-Centrosymmetric Crystals of Substituted Aliphatic Secondary Amines

[Bojidarka Ivanova](#) *

Posted Date: 23 January 2025

doi: 10.20944/preprints202501.1764.v1

Keywords: Organic photonics; non-centrosymmetric crystals; aliphatic secondary amines; chemical crystallography; quantum chemistry.



Preprints.org is a free multidisciplinary platform providing preprint service that is dedicated to making early versions of research outputs permanently available and citable. Preprints posted at Preprints.org appear in Web of Science, Crossref, Google Scholar, Scilit, Europe PMC.

Copyright: This open access article is published under a Creative Commons CC BY 4.0 license, which permit the free download, distribution, and reuse, provided that the author and preprint are cited in any reuse.

Article

Linear and Nonlinear Optical Properties of Non-Centrosymmetric Crystals of Substituted Aliphatic Secondary Amines

Bojidarka Ivanova

Lehrstuhl für Analytische Chemie, Institut für Umweltforschung, Fakultät für Chemie und Chemische Biologie, Universität Dortmund, Otto-Hahn-Strasse 6, 44221 Dortmund, Nordrhein-Westfalen, Germany; e-bojidarka.ivanova@yahoo.com or b_ivanova@web.de or bojidarka.ivanova@yahoo.com

Abstract: This paper like contributions to leading developments of nonlinear optical materials research aims for interdisciplinary readership and recognizing experimental and theoretical crystallographic, linear and nonlinear optical properties of non-centrosymmetric crystals of substituted aliphatic secondary amines as prospective templates for technological application. It deals with crystal structure of (2-piperazin-1-yl-ethyl)-nitrimine dihydrate (1) reported first, herein, that can be solved into both the P-1 and P1 space groups and 3,3,5-trimethyl-5-((nitroamino)methyl)cyclohexanaminium hydroxide (2) that could be solved into Pc and Pca₂₁ ones. Crystals of (1) and (2) exhibit optical transparency within 190–1100 nm. Comparative analysis with data on novel crystal structure of (2-piperazin-1-yl-ethyl)-carbamic acid dihydrate (3) is also carried out. There is utilizes high resolution single crystal X-ray diffraction, high accuracy quantum chemical methods for in-depth understanding of relation among molecular and crystal structures, crystallographic packing, symmetry, linear optical and nonlinear optical properties. There are also used electronic and Fourier transform infrared vibration spectroscopy. Organic material research might provide evolutionary development in the face of innovative change of photonics technologies. The research effort, so far, has shown that they are mainly rigid crystals. However, future photonics technologies mandate organic flexible devices; thus, opening research avenue for implementation of organic photonics and electronics devices.

Keywords: organic photonics; non-centrosymmetric crystals; aliphatic secondary amines; chemical crystallography; quantum chemistry

1. Introduction

The field of nonlinear optical (NLO) materials research has witnessed tremendous development over the recent decades as a result from their implementation into a broad spectrum of emerging technologies; for instance, lasers; light emitting diode ones; solar cell technologies; fiber-optic communications; nonlinear optical devices; pyroelectric detectors; memory devices; and, more. A number of NLO data-tables containing parameters of multi-functional materials have been developed (2023) [1]; thus, not only introducing innovative materials, but also allowing for their better comparison; property interpretation; and application-oriented characteristics among various developed bulk-materials; corresponding 0D–3D ones; metamaterials; on-chip, fiber, or hybrid wave-guiding materials [1–3]. Among, NLO parameters that should be considered, there are second-order nonlinear electrical susceptibility $\chi^{(2)}$; the effective second-order nonlinear coefficient d_{eff} ; and third-order nonlinear susceptibility $\chi^{(3)}$ [1,4]. There are highlighted a set of best practices specific and broadly used to discuss the research on the discussed field, as well. The study of second-order wave mixing processes of materials, emphasizing on second-harmonic generation (SHG) properties, amongst others, are frequently applied. Moreover, the second-order nonlinear optical spectroscopies, not only SHG one, but also sum frequency generation spectroscopy or linear electro-optic (Pockels)

effect are applicable to study not only bulk materials, but also their surfaces and interfaces [4–7]. Due to well-developed experimental methods for studying these processes detail on $\chi^{(2)}$ and d_{eff} coefficients are of importance in developing of innovative molecular templates for application-oriented aspects of the nonlinear optics.

However, both the SHG and Pockels effect as nonlinear frequency doubling processes arising due to $\chi^{(2)}$ ($(-2\omega, \omega, \omega)$ or $\chi^{(2)}(-\omega, \omega, 0)$) and strong second-harmonic signals — the same is valid to higher order NLO responses — could be observed only from non-centrosymmetric crystals [4,8–10].

Therefore, the development of the crystal engineering and design of single crystalline materials together with the comprehensive understanding of the connection among molecular structure, crystals structure, and both the linear optical and nonlinear optical properties of materials contribute crucially to develop a set of innovative and emerging NLO-technologies. The symmetry of the crystals in the later context plays a crucial role in design and tuning of optical properties of materials. The symmetry group of crystals defines the degrees of degeneracy of the corresponding energy levels of materials and governs selection rules for their electronic and vibronic transitions, respectively, observable optical phenomena. The crystal symmetry itself is governed chiefly by molecular packing of neutral species, respectively, ions in the crystal lattice of materials together with external factors and parameters such as crystallizing solvents, temperature, pressure, and more [11,12].

Further: The SHG phenomenon is sensitive toward crystalline surface and interface states, as well [13]. Thus, it could be observed in centrosymmetric crystals, when there is breaking of inversion symmetry of materials at the boundary.

In addition, assessment of effective non-linearity or d_{eff} coefficient of material is performed depending on space group type; thus, defining dielectric tensor ϵ_{ij} component and principal values of refractive indices [14]. The dielectric constants of crystals is useful parameter establishing the dielectric behavior of corresponding materials and assessing its polarizability; and, thus, SHG efficiency, because of high value of dielectric constant at low frequency could be a result from presence of all polarizations.

Conversely, a low value of dielectric constant at higher frequencies could be a result from gradual loss of all polarizations. In cases of low value of dielectric constant of the material in the higher frequency region could cause for enhancing SHG efficiency of grown crystalline material.

Furthermore, there could be variation depending on temperature. At low temperature, there is perturbation of SHG response due to crystal expansion in addition to expansion of electronic and ionic polarizations.

Conversely, the variation of SHG response at high temperatures is attributed to thermally generated impurity dipoles and charge carriers.

For the purpose of the current study, the effect of temperature on theoretical NLO-properties of crystals is accounted for relations shown in [15].

Thus, fabrication of novel NLO devices also involves knowledge of material dielectric constant, which is property of constituent ions of crystals in addition of data on electronic and ionic polarizabilities, and deformation of (counter)ions of crystals. Together with dielectric constant data on crystals, their refractive indexes, and electronic polarizability components, plasma energy, Penn gap, an Fermi energy used to analyze SHG phenomenon of crystals, [16]; data on first hyperpolarizability tensor components (β_{ijk}) are of significant importance for design and synthesis of novel NLO materials, because of NLO susceptibility $\chi^{(2)}$ is functionally related with them [4].

Perhaps, a strong argument, amongst others, favoring complementarily utilization of chemical crystallography and computational quantum chemistry for in-depth understanding of linear optical and nonlinear optical properties of crystals of organics, metal-organics, organometallics, or inorganics is that found within the so-called effective medium theory maintaining bridge between macroscopic properties of materials and corresponding microscopic response of their constituents such as molecules or ionic species of both of these upon effect of electromagnetic irradiation [17,18]. The high accuracy methods of computational quantum chemistry allow for determining dipole moment ($\mu_{g,i}$), polarizabilities, and hyperpolarizabilities (α_{ij} , β_{ijk} , and γ_{ijkl}) of materials; thus, usefully

helping to provide guidance for design and further optimizing of properties [4], because of these parameters estimate the corresponding macroscopic NLO phenomena; for instance, NLO susceptibility $\chi^{(2)}$. In order to facilitate a comparative analysis between theoretically calculated microscopic frequency-dependent first hyperpolarizability $\beta(-2\omega, \omega, \omega)$ (or SHG) or frequency dependent electro-optic Pockels hyperpolarizability $\beta(-\omega, \omega, 0)$ with SHG experiments there is frequently estimated SHG intensity which is determined via macroscopic second-order susceptibility, $\chi^{(2)}$ there is used using equations (1)–(4) [19]. The V denotes volume. (Consider equations (B2)–(B5) in Appendix B [19].) A simplistic presentation of equations (1)–(4) has been used to these purposes, as well [20]. The current study utilizes crystallographically determined volume data on crystals (1) and (2) as summarized in **Table 1** (below). The validation of theoretically computed relation of SHG via $\beta(-2\omega, \omega, \omega)$ hyperpolarizability and frequency dependent electro-optic Pockels hyperpolarizability $\beta(-\omega, \omega, 0)$ are comprehensively discussed [19,21]. The connection between Pockels and SHG effects is estimated via dispersion relations for diagonal components of electronic hyperpolarizabilities derived by Bishop and De Kee [22,23]. Useful definitions and fundamental relations used to this study can be found [24,25], as well.

$$\chi_{xzz}^{(2)}(-\omega; \omega, 0) = \frac{2 \times \pi}{V} \times \beta_{xzx}(-\omega; \omega, 0) \times \epsilon_{zz}(\omega) \times \epsilon_{zz}(0) \quad (1)$$

$$\chi_{zzx}^{(2)}(-\omega; \omega, 0) = \frac{2 \times \pi}{V} \times \beta_{zzx}(-\omega; \omega, 0) \times \epsilon_{zz}(\omega)^2 \quad (2)$$

$$\chi_{xzz}^{(2)}(-2\omega; \omega, \omega) = \frac{2 \times \pi}{V} \times \beta_{xzz}(-2\omega; \omega, \omega) \times \epsilon_{zz}(\omega)^2 \quad (3)$$

$$\chi_{zzx}^{(2)}(-2\omega; \omega, \omega) = \frac{2 \times \pi}{V} \times \beta_{zzx}(-2\omega; \omega, \omega) \times \epsilon_{zz}(2\omega) \times \epsilon_{zz}(\omega) \quad (4).$$

Further: There is not only breaking of space-inversion symmetry of crystals, but also breaking of time-inversion symmetry due to long-range magnetic ordering of species [13]. In the later case an applied magnetic field causes for novel contributions to SHG response. The effort on comprehensively classifying SHG phenomena in cases of magnetically ordered materials allows for an in-depth understanding of relation between the discussed phenomenon and magnetic structures of the materials.

However, the achieving of the latter goal is regarded as still elusive (2023) [8]. So far, it is well-established the fact that observable SHG effect indicates breaking of inversion symmetry of crystalline materials within the framework of electric-dipole approximation [8]. The latter approximation determines that a second order NLO process; if any, is forbidden in crystals with inversion symmetry [5]. However, as aforementioned, often, the symmetry is broken at the surface and interface of materials; thus, allowing, observation of SHG effect.

Owing to the fact that non-centrosymmetric space group type of crystalline materials appears prerequisite for a plausible both theoretical and experimental research of nonlinear optics, there should be a reliable justification of crystallographic structural solution depending on space group types. The reliability of crystallographic data is to be gauged via single crystal X-ray diffraction performances depending on space group types of structural solution and in accordance with a set of statistical criteria. However, frequently there are questions about specifics in applying the various methods for assessment of reliability of structural crystallographic solution, because of the quality of data depends not only on capability of statistical approaches used to chemical crystallography, but also on quality of single crystalline objects, its size, and scattering capability (consider detail on [15,26].) Despite the fact that many of these specific questions are already dealt with there are further reasons for questioning criteria for justification of structural solution, which cause for current debates, as well.

One of the most ubiquitous problems of crystal structure analysis of non-centrosymmetric crystals is ambiguity between centrosymmetric and non-centrosymmetric space group type, particularly, highlighting pairs $P1/P\bar{1}$; $P2_1/P2_1/m$; $C2/C2/m$; $Cc/C2/c$; and, $Pna2_1/Pnma$, among others [27–30]. The

crystal structure could contain centrosymmetric packing of molecules exclusively or there could be an equal amount of enantiomers. In the latter case there is cancellation of polarity in packing in non-centrosymmetric space group types. Due to these uncertainties between space group types there is recommended description of structures in centrosymmetric packing when there is a lack of supportive evidence for a corresponding non-centrosymmetric space groups [27–30]. On the other hand, there could be doubt about sufficiency of supportive evidences, as well as, because of a comprehensive analysis of available crystallographic data on Cambridge Crystallography Database Center (CCDC) performed by Marsh (1999) has shown that at about 21.5 % of crystal structures solved as triclinic non-centrosymmetric P1 space group are incorrectly solved and in fact correspond to compounds exhibiting centrosymmetric P-1 space group [31]. It has been highlighted that this is most common type of error occurring for crystals having triclinic space system. For the purposes of the current study it should be also underlined that structural solution depending on the space group types even looking at triclinic space system having only two space group types affects on geometry parameters and intermolecular distances of species; thus, affecting on theoretically predicted NLO-properties. It has been shown that when applied to space group P-1 rather than P1 one, then, this leads to reasonable intermolecular distances and to apparently reliable structures [31]. The reader should be well-awared as aforementioned that reliability of knowledge of relationship of crystal structure and nature of chemical bond, respectively, intermolecular interactions of crystals is of significant importance in development of the field of NLO materials research because of, so far, there is accumulated a large number of data on crystalline materials having ample reason to be self-confident that; for instance, organic crystals with predominantly ionic character of bonds between crystalline structural motifs or predominantly van der Waals interactions are among most prominent candidates for NLO organic Raman lasing materials [12,32]. From the perspective of major goal of this study it should be further highlighted that the shown above space groups are among the frequently found ones of NLO-materials. Particularly, the prospects of crystals exhibiting space group type P1 as prominent candidates for SHG green lasers has been highlighted [33]. Further, there could be mentioned stilbazolium salts as DSNS-1, DSNS-2, and DSDMS ones (p. 100 [4]) crystallizing also into P1 space group and showing prospective NLO-phore properties.

Despite, the fact that the field of NLO materials research chiefly elaborates innovative molecular templates of inorganics, the design and synthesis of novel organic compounds possessing large NLO properties shows prospective applications to NLO-technologies, spectroscopy, and integrated optics as photonic devices, frequency modulators, parametric oscillators, devices for data transmission, and mode, due to a set of advantages comparing with inorganic materials. For instance, these are easy design and modeling of novel materials via chemically controlled synthesis of structural selected modifications or changing of selected substituent or functional group of chemicals [33,34]. There should be also added advantages such as their low molecular weight, eco-friendly nature, and low cost [2,11,35–41].

Therefore, the concept of complementary application of chemical crystallography and computational quantum chemistry to estimate NLO-phenomena of organic crystals is involved, herein, to characterize molecular and crystal structure of (2-piperazin-1-yl-ethyl)-nitrimine dihydrate (1) (**Figure 1**) accounting for effect of crystallographic packing of both the space groups P-1 and P1 of the triclinic space system. A comparative analysis with crystals of 3,3,5-trimethyl-5-((nitroamino)methyl)cyclohexanaminium hydroxide (2) solved into monoclinic Pc and orthorhombic Pca₂₁ space groups is performed accounting for the fact that the latter non-centrosymmetric orthorhombic space group type belongs to among most favorable ones for design of novel NLO materials as aforementioned, but also as there has been highlighted above it is among the widely disputable one among the shown pairs of space groups of crystals [27–30]. The electronic absorption and vibrational properties of crystals of (1) and (2) are first detailed on this study both experimentally and theoretically. The latter data are further compared with novel crystallographic and optical spectroscopic results from synthetic derivative (2-piperazin-1-yl-ethyl)-carbamic acid dihydrate (3). The presented crystals are based on chemically substituted aliphatic secondary amines. They are

regarded as prospective templates for design and synthesis of organic NLO-phores, due to known facts, so far, showing that single crystals of such derivatives exhibit noble physico-chemical properties, lower cut-off wavelength, hardness, and high NLO efficiency (2024) [42–47] in addition to the fact that their polyproton accepting capability make them excellent templates for easily tunable crystallographic packing depending on experimental conditions and presence of counterions. It should be also add that the discussed class of organics, particularly, highlighting their nitrimines and carbamates have one-step synthetic scheme in mild synthetic conditions. A set of carbapates of studied herein aliphatic secondary amines; for instance, tert-butyl 4-(2-(methylamino)ethyl)piperazine-1-carboxylate [48], and (2-morpholin-4-yl-ethyl)-carbamic acid tert-butyl ester [49] (2020, 2022) have been reported. The discussed class of organic compounds is also broadly used to design of hybrid organic-inorganic NLO-phores; thus, exploring advantages of both the organic and inorganic constituents of crystals [43]. In the brief space of this paper it could be only further sketched some pro-arguments for advancing the discussed crystals (1) and (2) as prospective materials for applications to nonlinear optics. These derivatives show optical transparency within a broad range of electromagnetic spectrum encompassing 190–1000 nm; and, importantly, these compounds preferable crystallize into non-centrosymmetric space group types. The carbamate-derivative (3) can be produced via simple non-isocyanate route, as well. It is developed as mild synthetic approach to polymer research yielding to aliphatic thermoplastics [50]. Owing to the fact that the latter method is applied to 3-aminomethyl-3,5,5-trimethylcyclohexylamine, however; thus, obtaining polymer material instead of short chain oligomers the nitrimine chemical substitution of crystals (1) and (2) appears preferable approach; thus, avoiding the easy polymerization processes of the discussed analytes, particularly, highlighting the 3-aminomethyl-3,5,5-trimethylcyclohexylamine. The refractive index of the latter compound is 1.4888 at $T=20^{\circ}\text{C}$ and $\lambda=589$ nm [51,52], while aminoethylpiperazine the refractive index is 1.5298 at $\lambda=589$ nm and $T=20^{\circ}\text{C}$ [53]. The theoretical analysis of optical and nonlinear optical properties involves linear optical and frequency dependent nonlinear optical characteristics of the crystals with respect to the different space groups in gas-phase and polar media together with the study of the effect of the temperature on the nonlinear optical properties.

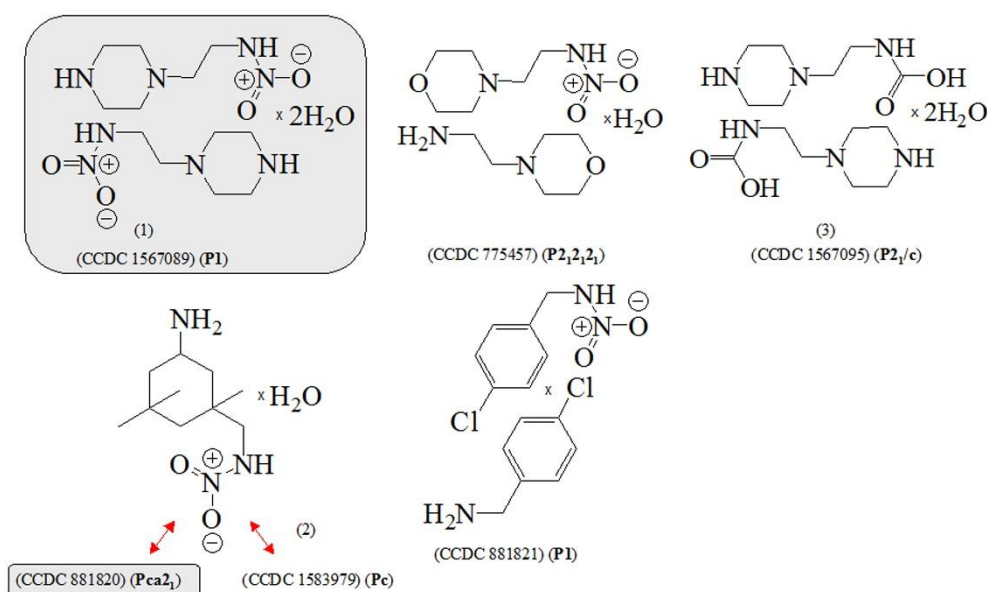


Figure 1. Chemical diagrams of crystals presented and discussed in this study; CCDC codes, and space group types; crystal structures of (2-piperazin-1-yl-ethyl)-nitrimine dihydrate (1) (CCDC 1567089) and (2-piperazin-1-yl-ethyl)-carbamic acid dihydrate (CCDC 1567095) (3) are reported first, herein, while only crystallographic data on structural solutions of 3,3,5-trimethyl-5-((nitroamino)methyl)cyclohexylamine hydroxide (2) into space groups Pc (CCDC 1583979) and Pca2₁ (CCDC 881820; polymorph I) are according to [54–56]; crystallographic data on 2-(morpholin-4-yl)-N-nitroethanamine 2-(morpholin-4-yl)ethanamine monohydrate (CCDC 775457)

[55,57] and 1-(4-chlorophenyl)-N-nitromethanamine 1-(4-chlorophenyl)methanamine, [55,58] have been reported, previously; data on non-centrosymmetric (Pca2₁) polymorph II of N-((5-amino-1,3,3-trimethylcyclohexyl)methyl)nitramide monohydrate have been reported to [59,60].

2. Materials and Methods

2.1. Synthesis

The synthesis of (1) was performed by non-substituted 2-piperazin-1-yl-ethylamine base (Sigma-Aldrich Inc., 0.1291 g) with nitric acid under heating at T=100°C for t=2h. The utilization of slow-evaporation approach to the mixture causes for isolating of colorless single crystals at about a week. Yields 60%. Analytical calculations for [C₆H₆N₄O₃] (1): C, 37.49; H, 8.39; N, 29.15 %. Found (1): C, 37.50; H, 8.13%. The synthetic scheme is applicable to other aliphatic secondary amines, as well [55,59].

Further: References [54]–[60] detail on crystallographic data on species depicted in **Figure 1** excluding from the novel crystals (1) and (3) reported to this study, first. The same is valid to optical spectroscopic data on crystal (2) which are also reported for the first time in the literature in the current paper. Both the vibration spectroscopic and mass spectrometric data on polymorphs I and II of the orthorhombic phase Pca2₁ of (2) have been detailed on [59]. The latter study details on the experimental crystallographic and theoretical electron density analysis of (2), as well.

2.2. Analytical Instrumentation

The single crystal X-ray diffraction hkl-intensities of crystals were obtained using Bruker Smart X2S diffractometer, and micro source Mo Ka radiation. There was employed ω scan operation mode. The structural data-blocks of crystallographic variables were processed by SHELXS-97 [61–63], OLEX2 [64], and PLATON [65], respectively. Crystallographic refinement parameters are listed in **Tables 1** and **S1**. The crystal structures of (1)–(3) are presented via PLATON [66] (**Figure 2**). The applied absorption correction method is based on multiple scanned reflections. The crystal structures were solved by direct methods using SHELXS-97 and were refined by full matrix least-squares refinement against F² [61–63]. Anisotropic displacement parameters were introduced for all non-hydrogen atoms. The experimental structural factors were further processed by WinGX 2014 [67] towards data quality. WTANAL and DRK plot analyses of the structure factors were carried out. In addition, to residual analyses and THMA were performed; thus, evaluating the thermal motion on the basis of the experimentally measured U_{ij} values [68,69].

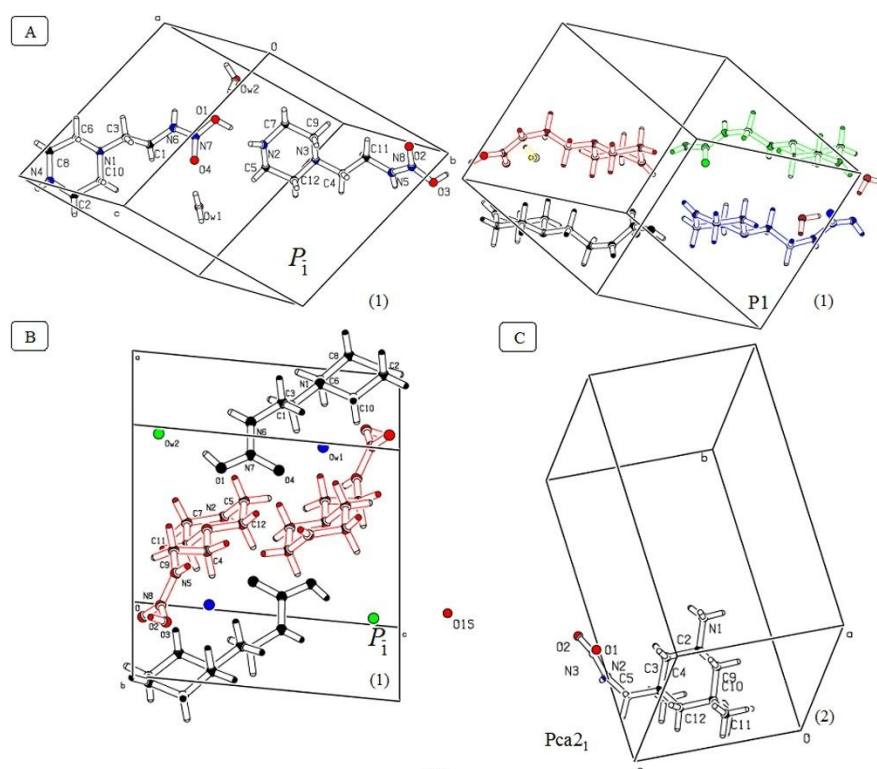


Figure 2. PLUTON plot of unit cell content of crystal (1) depending on the space group type P-1 to P1 (A); packing structure of crystal (1) in space group P-1 (B); asymmetric unit of crystal (2) in Pca2₁ space group (CCDC 881820 [55,56]) (C).

HPLC–ESI-tandem MS/MS measurements were performed on TSQ 7000 instrument (Thermo Fisher Inc., Rockville, MD, USA), using mobile phase compositions 0.1% (v/v) aqueous solution of HCOOH, 0.1% (v/v) HCOOH in CH₃CN; 20.0% (v/v) HCOOH in CH₃CN:CH₃OH solvent mixture 1:1; and 10.0% KOH/NaCO₃ in CH₃OH. A triple quadrupole mass spectrometer (TSQ 7000 Thermo Electron, Dreieich, Germany) equipped with an ESI 2 source was employed for ESI-MS measurements under experimental conditions shown in [55]. The mass spectrometric data were processed by Excalibur 1.4 software. A standard LTQ Orbitrap XL (Thermo Fisher Inc.) instrument was employed, as well. The chromatographic analysis was performed with a Gynkotek (Germering, Germany) HPLC instrument, equipped with a preparative Kromasil 100 C18 column (250x20 mm, 7 µm; Eka Chemicals, Bohus, Sweden) and a UV-detector set at 250 nm. The mobile phase is CH₃CN:H₂O (90:10, v/v) at a flow rate of 4 mL.min⁻¹. The analytical HPLC was performed on a Phenomenex (Torrance, CA, USA) RP-18 column (Jupiter 300 150x2 mm, 3 µm) under the shown conditions. The analysis was carried out using Shimadzu UFLC XR (Kyoto, Japan) instrument, equipped with an auto-sampler, PDA, an on-line degasser and column thermostat. As stationary phase a Phenomenex Luna Phenyl-Hexyl column (150x3mm i.d., 3 µm particle size) was used.

The IR-spectra were measured on a Bomem Michelson 100 FTIR spectrometer (4000–400 cm⁻¹, ±1 cm⁻¹ resolution, and 200 scans). It is equipped with a Specac wire-grid polarizer. The data were processed via GRAMS AI 7 software (Thermo Fisher Scientific Inc.)

The UV–VIS–NIR spectra were recorded on Evolution 300 spectrometer within the 190–1100 nm range.

2.3. Theory/Computations

The GAUSSIAN 98, 09; Dalton2011 and Gamess-US [70–72] program packages were used. The output files were visualized by GausView03 [73]. Ab initio and DFT molecular optimization was carried out by means of B3LYP, B3PW91 and ωB97X-D methods, respectively. The Truhlar's functional M06-2X was used, as well [74,75]. The algorithm by Bernys was taken into determine the

ground state. The stationary points at the potential energy surface (PES) were obtained by harmonic vibrational analysis. The criterion confirming minima of the energy is the absence of imaginary frequencies (negative eigenvalues) of second-derivative matrix. The basis set cc-pVDZ by Dunning, 6-31+ + G(2d,2p), quasirelativistic effective core pseudo potentials from Stuttgart-Dresden(-Bonn) (SDD,SDDAll, <https://www.cup.uni-muenchen.de/oc/zipse/losalamos-national-laboratory-lanl-ecps.html>), and LANL2DZ were used [76]. The zero point vibrational energy and vibrational contributions have been accounted for up to a magnitude value of 0.3 eV. Species in solution were examined by of explicit super molecule and “mixed” approach of micro hydration. The polarizable continuum method is used. The effect of the ionic strengths in solution was accounted for integral-equation-formalism polarizable continuum model. Merz-Kollman atomic radii and heavy atoms UFF topological models were used. Large species were treated using own N-layer integrated molecular orbital and molecular mechanics method. The electrostatic potentials and natural bond orbital (NBO) methods are applied, as well. The molecular dynamics was performed by ab initio or DFT Born Oppenheimer approach. It was also carried out at M062X functional and SDD or cc-pvDZ basis sets, without to consider periodic boundary condition. The trajectories were integrated using Hessian-based predictor–corrector approach with Hessian updating for each step on Born – Oppenheimer potential energy surface. The step sizes were 0.3 and 0.25 amu/Bohr. The trajectory analysis stops when: (a) centers of mass of a dissociating fragment are different at 15 Bohr, or (b) when the number of steps exceed the given to as input parameter maximal number of points. The total energy was conserved during the computations within at least 0.1 kcalmol⁻¹. The analysis was performed by fixed trajectory time speed (*t* = 0.025 or fs) starting from initial velocities. The velocity Verlet and Bulirsch-Stoer integration approaches were used. The Allinger’s molecular mechanics force field MM2 was also employed [77]. The low order torsion terms is accounted with higher priority rather than van der Waals interactions. The accuracy of the method comparing with experiment is 1.5 kJ.mol⁻¹ studying diamante [78]. The differences in heats of formation of alcohols and ethers is |0.04|–|6.02| kJ.mol⁻¹.

Crystallographic structural data on (1) and (2) were used to input atomic coordinates during quantum chemical computations.

Calculations of electron absorption spectra were performed using exchange correlation potential and including scalar-relativistic effects. The electronic absorption spectra were obtained by electronic excitation computations within linear response in time dependent density functional theory and the Tamm–Dancoff approximation [79–81].

Table 1. Crystallographic refinement data on crystals (1) and (2); data on crystal (3) are shown in **Table S1**; the non-centrosymmetric solution of (1) is presented as supporting information (s.i.).

Compound	(1)		(2)		
CCDC	1567089	(s.i.)	1583979	881820	1583979
				Polymorph I	Polymorph II
Ref.	This study	This study	[54,55]	[55,56]	[59,60]
Empirical formula	C ₆ H ₁₅ N ₄ O ₃	C ₆ H ₁₅ N ₄ O ₃	C ₁₁ H ₂₂ N ₃ O ₃	C ₁₁ H ₂₂ N ₃ O ₃	C ₂₀ H ₃₄ N ₆ O ₆
Moiety formula	C ₆ H ₁₅ N ₄ O ₃	C ₆ H ₁₅ N ₄ O ₃	C ₁₁ H ₂₂ N ₃ O ₃	C ₁₁ H ₂₂ N ₃ O ₃	C ₂₀ H ₃₄ N ₆ O ₆
Formula mass	191.22	191.22	244.32	244.32	454.53
Crystal system	Triclinic	Triclinic	Monoclinic	Orthorhombic	Orthorhombic
Space Group	P-1	P1	Pc	Pca2 ₁	Pca2 ₁
<i>a</i> [Å]	9.646(2)	9.646(2)	7.9820(18)	10.9481(15)	10.951(2)
<i>b</i> [Å]	10.321(2)	9.646(2)	14.438(3)	14.463(3)	28.852(6)

c [Å]	11.047(3)	10.321(2)	10.9433(19)	8.0063(12)	7.9923(18)
α [°]	108.944(6)	11.047(3)	90.00	90.00	90.00
β [°]	95.120(7)	108.944(6)	90.00	90.00	90.00
γ [°]	105.960(6)	105.960(6)	90.00	90.00	90.00
V [Å ³]	980.7(4)	790.6(3)	1261.1(5)	1267.8(3)	2525.2(9)
Z	4	4	4	4	4
ρ [g.cm ⁻³]	1.282	1.190	1.287	1.217	1.196
F000	408	378	532	508	976
ρ(Mo-K) [mm ⁻¹]	0.100	0.095	0.094	0.090	0.089
T [K]	293(2)	199(2)	199(2)	198(2)	199(2)
ρ range	2.59–25.07	2.59–25.07	2.55–24.76	2.33–25.04	2.33–25.04
Refl. collected	3395	9254	7635	7565	4281
Unique refl.	2602	6569	3544	2223	3415
R1[2σ(I)]	0.1127	0.1060	0.0515	0.0617	0.1224
R1 (all data)	0.3194	0.3313	0.1254	0.1548	0.3277
wR2	0.1305	0.1306	0.0699	0.0804	0.1659
GooF	2.151	1.274	1.139	0.985	1.479
Diff. peak/ hole [e/Å ³]	0.854/-0.574	0.898/-0.590	0.222/-0.358	0.278/-0.398	1.517/-0.885

3. Results

3.1. Crystallographic Data

Figure 2 depicts unit cell content and packing of crystal (1) solved into both the triclinic P1 and P-1 space groups. The application of ADDSYM test to these structural solutions (**Figures S1 and S2**) indicates that there should be favored the latter one, despite, the fact that the non-centrosymmetric solution of the crystal yields to lower performances and R₁ factors (R₁=0.1060). **Figure S3** illustrates powder X-ray diffraction data. The ensemble of two organic molecules of packing of the centrosymmetric phase and the unit cell content of the non-centrosymmetric one of (1) show similar intramolecular interaction networks (**Figure 3.**) There is slide variation of NOH...NH, NH...ON, and HOH...OHN bonds showing parameters r(O...N)=2.681, r(N...O)=2.757, and r(O...O)=2.852 Å of P-1 crystal of (1) and r(O...N)=2.679, r(N...O)=2.665, and r(O...O)=2.752 Å of its non-centrosymmetric P1 phase.

The application of ADDSYM test of structural solutions of crystal (2) in Pc and Pca2₁ space group types (**Figures S4 and S5**) indicates that there is favored the non-centrosymmetric orthorhombic Pca2₁ space group type showing Z=4 or one organic molecule in the unit cell. The asymmetric unit of (2) is shown in **Figure 2C**. The molecules of (2) are involved into moderate NH...O interactions (r(N...O)=2.814–2.835 Å); thus, forming a 3D intermolecular hydrogen bonding network. The test results from crystallographic solution of (3) are shown in **Figure S6**.

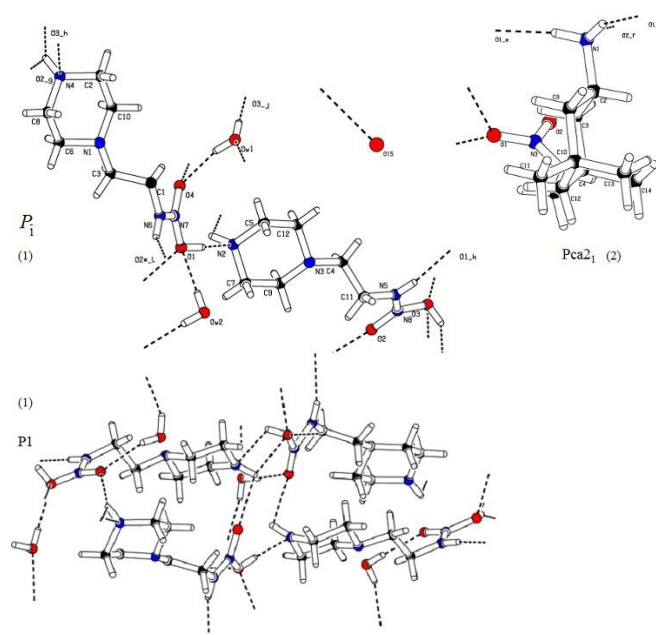


Figure 3. Intermolecular hydrogen bond networks of crystals (1) and (2) in P-1, P1, and Pca2₁ space groups; data on (2) are according to (CCDC 881820) [55,56].

3.2. Electronic Transmission Spectra

The electronic transmission spectra of (1) and (3) are shown in **Figure S7**. The former crystal (1) is transparent within 190–1100 nm; thus, making it suitable candidate for NLO-application. The low-intensive UV-bands of (3) are assigned to $n \rightarrow \pi^*$ and $\pi \rightarrow \pi^*$ transitions of carbamate structural sub-unit of the aliphatic secondary amine. **Figure S8** depicts corresponding data on Pca2₁ crystal of (2). Due to polyproton accepting capability of 3-aminomethyl-3,5,5-trimethylcyclohexylamine there is studied effect of pH on its optical properties. With increasing in pH, there is observed a band at 195.0 ± 0.52 nm assigned to charge transfer effect between the aliphatic secondary ammonium cation and inorganic counterion in the acidic medium.

3.3. Vibration Spectroscopic Data

The IR-spectrum of non-substituted 1-(2-aminoethyl) piperazine has been detailed in [82]. The data on its nitrimine and carbamate derivatives obtained in crystals of (1) and (3) are depicted in **Figure S9**. There is highlighted difference in IR-spectra of the two types of substituents consisting of intensive band at 1717 cm^{-1} of $\nu_{\text{C=O}}$ stretching vibration of carbamate moiety of (3). The obtained IR-spectroscopic patterns of crystals (1) and (3) agree well with results from powder X-ray diffraction (**Figure S3**) and scarce available vibrational spectroscopic characteristics of isophoronecarbamate showing IR-bands in liquid phase at 668, 738, 779, 866, 893, 954, 1017, 1043, 1069, 1139, 1154, 1193, 1251, 1311, 1343, 1365, 1387, 1463, 1542, 1696, 2848, 2922, 2954, 3069, and 3333 cm^{-1} [83] together with data on analogous derivative of morpholine revealing IR-bands at 2974, 2875, 1695, 1407, 1255, 1266, and 1128 cm^{-1} , respectively [84]. The presence of intensive band within $1720\text{--}1695 \text{ cm}^{-1}$ of $\nu_{\text{C=O}}$ stretching vibration appears characteristic mode of carbamate-derivatives of aliphatic secondary amines.

Figure 4 illustrates solid-state IR-spectrum of the non-centrosymmetric Pca2₁ phase of (2) together with the IR-pattern of the starting analyte 3-aminomethyl-3,5,5-trimethylcyclohexylamine. Since, the vibrational IR-spectroscopy appears a powerful approach to distinguish between nitrimine- and carbamate-derivatives of aliphatic secondary amines it has been already applied to such as derivatives in course of our systematic analysis of organic crystal of salts, including the second Pca2₁ polymorphs of (2) [59].

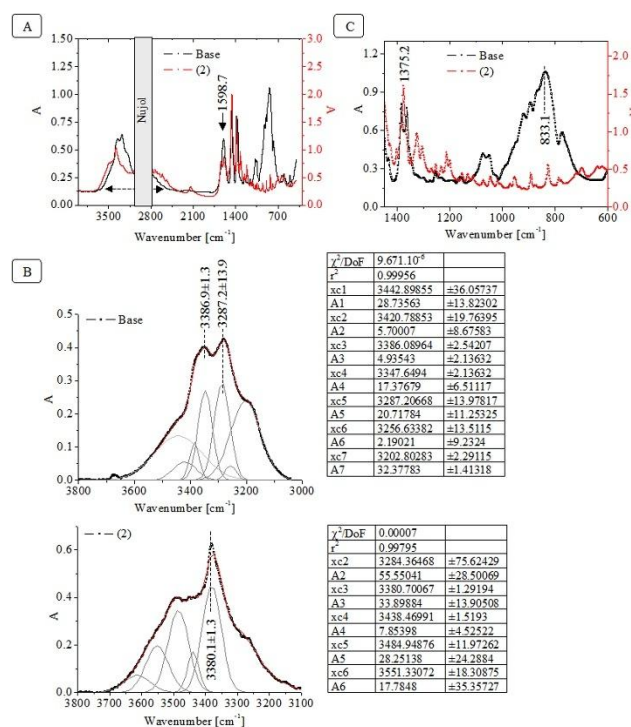


Figure 4. Condensed phase FT-IR spectra of crystal (2) in nujol mull and liquid 3-aminomethyl-3,5,5-trimethylcyclohexylamine (base) within different regions of the electromagnetic spectrum (A); curve fitted spectroscopic patterns of the two analytes within 3800–3000 cm⁻¹; chemometrics (B); the IR-spectrum of the non-substituted liquid base has been detailed on theoretically and experimentally in [59].

3.4. Theoretical Data

The α and β tensors obtained from the theoretical treatment are microscopic quantities that refer to a unit cell in crystals or to a single molecule in the 0D case [19]. The application of symmetry operations permits utilization of the discussed computations to periodic systems of crystals. Particularly inorganics crystallizing into non-centrosymmetric space group types Cmc2₁ and P1 of boehmite have been computed [85]. In our case there is Pca2₁ which belongs to the same orthorhombic point group 'mm2', using Hermann–Mauguin notation as Cmc2₁, while Pc and Cc belong to monoclinic point group 'm' according to the latter notation. Despite, the fact that in the case of crystal (2) there are comparable R_i-parameters of crystallographic solutions in both the monoclinic Pc (R_i=5.15) and orthorhombic Pca2₁ (R_i=6.17) space groups there is favor high symmetry [86]. For this reason, a large number of crystal structure prediction approaches utilize for input parameters guess structures that are of high space symmetry, due to the fact that the most similar low-energy structures; if any, could be found much more rapidly [86]. Due to reasons sketched, so far, there is used the unit cell content of crystals for purposes of the theoretical analysis or asymmetric units, which are smallest part of molecular crystal structure allowing for symmetry operations to obtain complete unit cell of the crystal, which is its repeating unit. The utilization of the asymmetric unit is carried out in the case of crystal (1) due to the following reasons. A survey of crystal structures in the chiral space group P1 has shown that the standard deviation of the structural solutions depending on the space group type, thus, distinguishing between P-1 and P1 ones away from inversion symmetry could be as low as 0.07 Å as in the case of (1) [31,87,88]. Due to these reasons there is slight as aforementioned variation between the unit cell content of the non-centrosymmetric phase of (1) and the packing one of its P-1 phase. As illustrated in the preceding sub-sections this fact causes for identical type of intermolecular hydrogen bonding network and slide variation of the geometry parameters. Therefore, these lies a reasonable question: How to distinguish between the two type of crystallographic packing of (1) depending on the triclinic space group types? As an effort to address

the latter question adequately there are computed two types of packing of molecules of the non-centrosymmetric P1 phase of (1) shown in **Figure 5**.

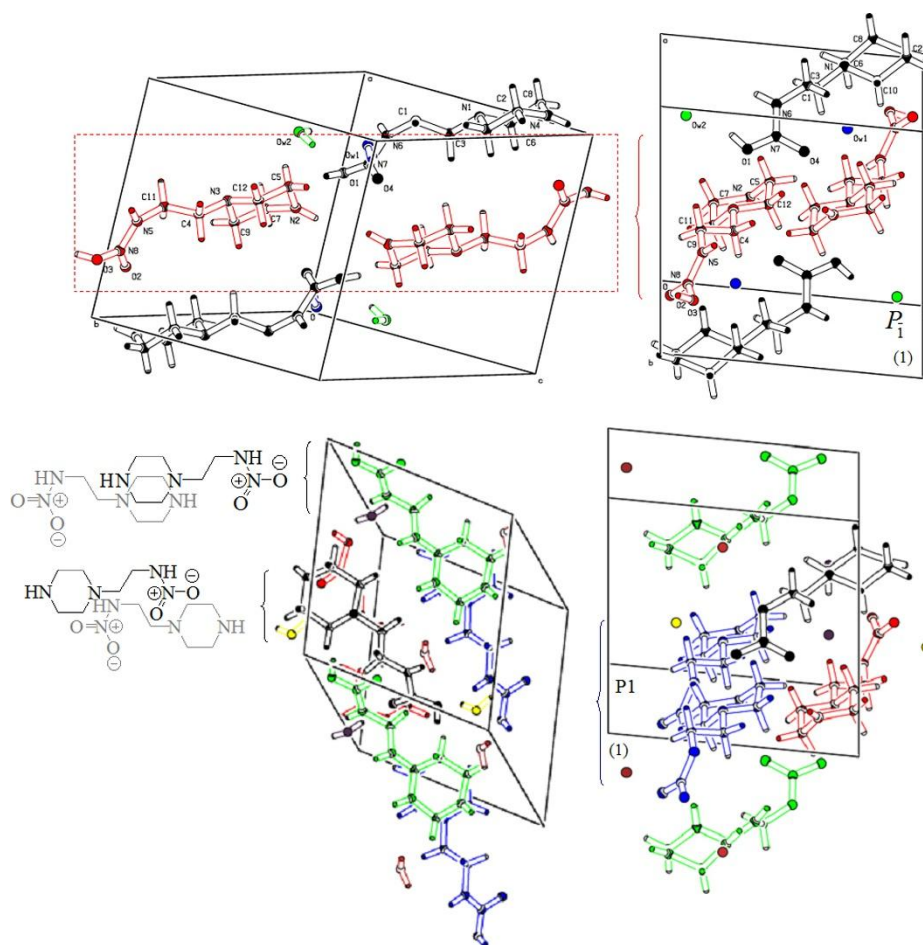


Figure 5. The unit cell content and packing of (1) depending on the space group type; chemical diagrams of ensembles of interacting pairs of molecules typical for only non-centrosymmetric phase P1 of the crystal of (1).

The reliability of theoretical analysis of NLO properties of crystals including NLO-ones and asymmetric unit has been illustrated comparing theoretical and experimental hyperpolarizability data on crystal of crystals of l-phenylalanine-l-phenylalaninium chloride [89,90]. The work [90] estimates experimental and theoretical SHG-data on bis(guanidinium) 2,2'-bipyridine-3,3'-dicarboxylate with respect to various ab initio and DFT approaches.

Figure 6, Tables 2, S2 and S3 summarize the theoretical NLO-data on crystals (1) and (2) depending on the space group type. There are computed and summarized different symmetry relations among tensor components of $\beta_{ijk}(-\omega; \omega_1, \omega_2)$, because of all they are obeyed studying NLO-materials.

Crystal (1) shows large polarizability and hyperpolarizability data comparing with crystal of (2); furthermore, accounting for a large difference in tensor component values, which could be attributed with the extended molecular geometry of the nitrimine derivative of 2-piperazin-1-yl-ethylamine comparing with the corresponding derivative of 3-aminomethyl-3,5,5-trimethylcyclohexylamine.

A comparative analysis with experimental SHG and theoretical dynamics hyperpolarizability data on guanidinium salt of 2,2'-bipyridine-3,3'-dicarboxylic acid crystallizing into orthorhombic space group Pca2₁ [90] as the crystal (2) reported, herein, it could be said that crystal (1) first presented in this paper shows 8.95, 1.18, and 1.72 times larger b_{xxx} , b_{xyy} , and b_{xzz} tensor component values comparing with the innovative organic NLO-phore reported to work [90]. The comparative analysis involved results from computations of unit cell content and the asymmetric unit as aforementioned. The same theoretical design has been applied to study [90]. In addition, there is obtained exact

polarizability of (1) $\alpha=429.511.10^{-24}$ esu in gas phase. The computations in polar protic solvet water show increasing in value up to $\alpha=704.366.10^{-24}$ esu. The latter results are in agreement with the statement that solute-solvent interactions of NLO-phores depending on the properties of the medium could dramatically modify the electronic NLO-response of solute species [91]. Despite, the fact that the latter work underlines the discussed effect as predominantly observable in conjugated push-pull organic NLO-phores, this study shows that the medium affect on NLO-performances of aliphatic secondary amines, as well. The dynamic polarizability data on (1) are comparable with results from *N*4,*N*4-dimethyl-2-(methylsulfanyl)-*N*6-(4-phenoxyphenyl)pyrimidine-4,6-diamine designed as innovative multifunctional material, including, organic NLO-phore (2024) [92].

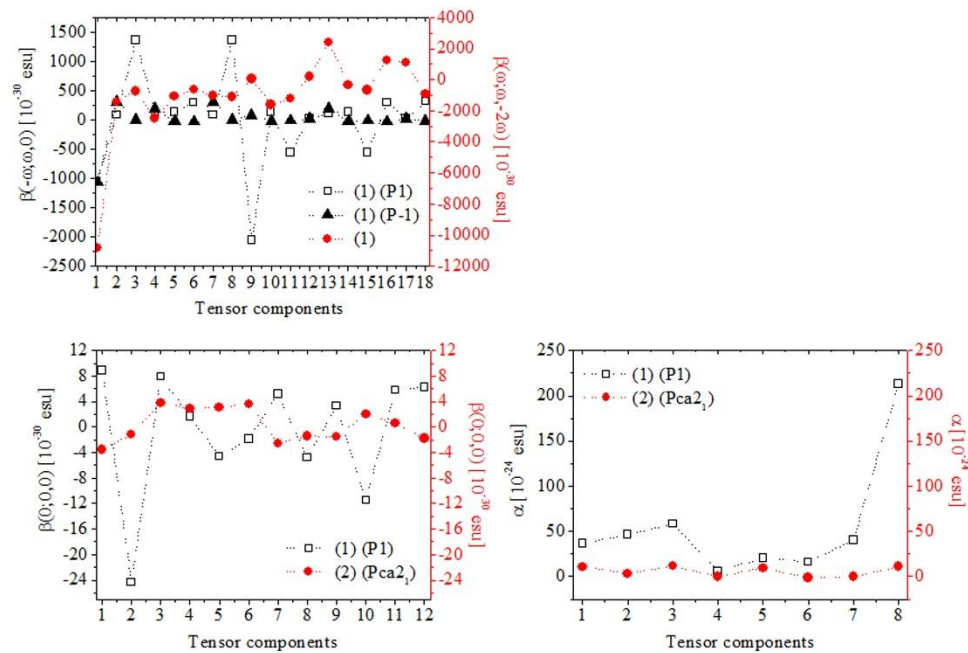


Figure 6. Dynamic nonlinear optical properties of the non-centrosymmetric phases P1 and Pca2₁ of crystals (1) and (2).

Table 2. Static and dynamic nonlinear optical properties of the non-centrosymmetric P1 phase of crystal (1); ||, ⊥ denote parallel and perpendicular components; (z) with respect to z axis; vector components x,y,z.

Electric dipole moment [Debye]		First dipole hyperpolarizability, β [$\cdot 10^{-30}$ esu]	
α_{tot}	$0.241711.10^1$		
α_x	0.0	$\beta_{ \parallel(z)}$	$0.884883.10^1$
α_y	0.0	$\beta_{\perp\perp(z)}$	$-0.243294.10^2$
α_z	$0.241711.10^1$	β_{xxx}	$0.792536.10^1$
Dipole polarizability, α [10^{-24} esu]		β_{xxy}	$0.160591.10^1$
α_{iso}	$0.367945.10^2$	β_{yxy}	$-0.456727.10^1$
α_{aniso}	$0.464008.10^2$	β_{yyy}	$-0.184039.10^1$
α_{xx}	$0.583943.10^2$	β_{xxz}	$0.521545.10^1$
α_{yx}	$0.607893.10^1$	β_{yxz}	$-0.478818.10^1$
α_{yy}	$0.204121.10^2$	β_{yyz}	$0.327977.10^1$
α_{zx}	$0.162562.10^2$	β_{zxx}	$-0.114679.10^2$
α_{zy}	$0.401414.10^2$	β_{zyz}	$0.579436.10^1$

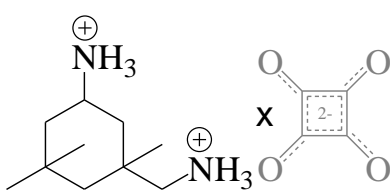
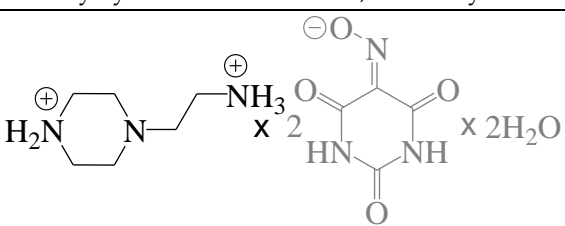
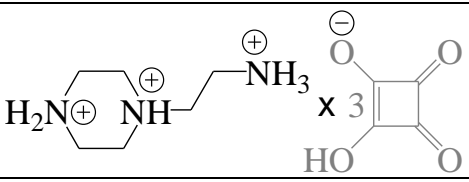
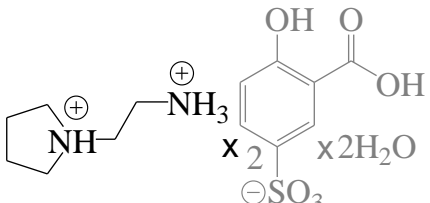
α_{zz}	$0.213094.10^3$	β_{zzz}	$0.625282.10^1$
$\alpha(-\omega;\omega) \omega=455.6 \text{ nm } [10^{-24} \text{ esu}]$		$\beta(-\omega;\omega,0) \omega= 455.6 \text{ nm}$	
α_{iso}	$-0.373816.10^2$	$\beta_{ (z)}$	$-0.425821.10^3$
α_{aniso}	$0.139823.10^3$	$\beta_{\perp (z)}$	$-0.184992.10^5$
α_{xx}	$-0.124242.10^3$	β_{xxx}	$-0.625373.10^4$
α_{yx}	$0.283544.10^2$	β_{yxx}	$-0.347627.10^3$
α_{yy}	$0.537980.10^1$	β_{yyx}	$-0.129018.10^3$
α_{zx}	$-0.400332.10^1$	β_{zxx}	$-0.624656.10^3$
α_{zy}	$0.614927.10^1$	β_{zyx}	$0.142934.10^3$
α_{zz}	$0.671765.10^1$	β_{zzx}	$0.535172.10^2$
		β_{xxy}	$-0.162021.10^4$
		β_{yxy}	$0.217864.10^3$
		β_{yyy}	$-0.584540.10^2$
		β_{zxy}	$0.355250.10^2$
		β_{zyy}	$0.329955.10^2$
		β_{zzy}	$-0.517619.10^2$
		β_{xxz}	$-0.780140.10^3$
		β_{yxz}	$-0.659689.10^{-1}$
		β_{yyz}	$-0.112060.10^2$
		β_{zxz}	$0.113699.10^3$
		β_{zyz}	$0.191883.10^2$
		β_{zzz}	$-0.514790.10^2$

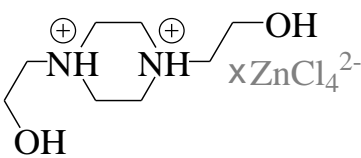
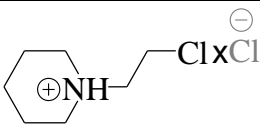
4. Discussion

After considering experimental and theoretical data on linear and nonlinear optical properties of non-centrosymmetric P1 and Pca2₁ phases of crystals (1) and (2) of nitrimines of aliphatic secondary amines the discussion seems to be forced into following direction. The inorganic materials are key crystalline templates for applications to photonics technologies including lasers [1]. Despite, organic-inorganic hybrid materials and organometallics have also garnered increasing attention (2025) as marked templates for design and development of innovative NLO-phores due to their significant structural flexibility; and stability; furthermore, allowing incorporation of a large scale of organic constituents as an effort to model effectively their NLO-performances [15,93–95]. The same is valid to organic NLO-phores due to richness in molecular structural templates; thus, providing a plethora of molecular properties and bonding mode possibilities of their crystals allowing easy tunable a broad spectrum of properties of such materials [96–99]. Particularly, the highlights are on the capability of incorporating chiral molecules are organic constituents; thus, breaking the symmetry of the bulk crystalline material and facilitating the formation of non-centrosymmetric space group type templates of materials, because of there are two important criteria for potential technological application of photonics crystal with highlighted SHG response consisting of (i) large first-order molecular hyperpolarizability parameters, and (ii) non-centrosymmetric space group type of the crystal structure [100,101]. The non-centrosymmetric crystals show second order NLO-features which are required for generating NLO-devices [102]. The former criterion is closely connected with the molecular structure of the constituents of the crystals and their electrical polarization properties. The latter criterion depends mainly from the molecular packing of the crystals [101]. The strategy used to design and synthesis of both the metal-organics or organic NLO materials is mainly

implemented into the field of crystal engineering of novel molecular structures exhibiting linear and NLO-properties, because of chiral molecules produce non-centrosymmetric crystals. However, in the light of the later statement it might well be said that there are observation statements that could be considered as important step of organization of research experience and development of effective strategies for production of innovative NLO-templates of both metal-organic and organic materials. They should be considered as an effort on optimizing efficiency of photonics crystals, because of the search of high performance crystalline templates has grown significantly looking at faster, efficient, and reliable and reliable innovative optical devices; thus, excluding from only approach to implement chiral constituents into the bulk crystals of materials, because of such compounds show frequently low quality crystal growth. The current study takes a view that the no chiral molecular templates could be also usefully implemented into the design of novel NLO-phores. The current study highlights the aliphatic secondary amines as such as molecular templates, particularly highlighting their nitrimines, despite, the fact that our systematic research effort on design and synthesis of organic salts of these derivatives has shown that often depending on the type of the counterion there are produced non-centrosymmetric crystals without implementation of chiral agents. Together with the crystal (1) reported to this study, first, there could be mention organic salts of the same aliphatic secondary amine, 2-piperazin-1-yl-ethylamine that produce diversity of non-centrosymmetric structures depending on the counterion. **Table 3** details on examples of our practice of non-centrosymmetric crystals of the latter analyte and structurally similar bases in addition to examples of primary amine 3-aminomethyl-3,5,5-trimethylcyclohexylamine used to design and synthesis of (2).

Table 3. Crystallographic data on selected non-centrosymmetric crystalline template of aliphatic amines of our systematic series of their crystals of organic salts and metal-organic materials.

CCDC	Space group	Chemical diagram	Ref.
760142	Pca2 ₁		[103,104]
(3-(ammoniomethyl)-3,5,5-trimethylcyclohexanaminium 3,4-dioxocyclobut-1-ene-1,2-diolate)			
882498	C2/c/Cc		[103,105]
9-aza-3,6-diazoniaspiro [5.5]undeca-2,8-diene bis(5-nitroso-2,6-dioxo-1,2,3,6-tetrahydropyrimidin-4-olate) monohydrate			
770390	P2 ₁ /P2 ₁ /c		[106,107]
2-(piperazine-di-ium-1-yl)ethylammonium tris(hydrogen squarate) monohydrate			
775456	P2 ₁ 2 ₁ 2 ₁		[108,109]

1-(2-ammonioethyl)pyrrolidinium bis(3-carboxy-4-hydroxybenzenesulfonate) trihydrate			
832306	Pca2 ₁ /Pmna		[110,111]
1,4-bis(2-Hydroxyethyl)piperazinedi-ium tetrachloro-zinc(ii)			
792094	Pca2 ₁ /Pmna		[112,113]
1-(2-chloroethyl)piperidinium chloride			

A this point, I should concentrate on the fact that these non-centrosymmetric crystals are obtained within the one step synthesis in mild conditions and high yields; thus, further allowing flexible design and chemical substitution. In addition there should be highlighted that these derivatives coordinate preferably with transition metal ions; thus, producing diverse metal-organic hybrid templates, as well (**Table 3**). The latter statement, particularly, is connected with the fact that a comprehensive study devoted to comparative theoretical analysis of dynamic NLO-performances of organics and corresponding metal-organic materials with the same organic ligands has shown that there is 1.37 – 1.12 [10-30 cm⁵.esu⁻¹] of b_{HRS} of the free ligands and their corresponding Zn^{II}-complexes [114]. Therefore, the in-depth study of the molecular factors affecting on NLO-properties of materials is directly connected with not only the development of the organic NLO-materials research, but also the metal-organic and organometallic one.

Therefore, the effective evaluation of the NLO-performances could be carried out focusing the attention on the first hyperpolarizability data among others [1,100,101] which accounts for the material response to an applied electric field. It is capable of generating second-order NLO effects [100,101]. The magnitude order depends on a set of factors; for instance, molecular structure and electronic properties of the molecules constituting the crystals, their symmetry, and more [100,101]. The latter knowledge could be tailored in order to enhance NLO performance. The complementary application of chemical crystallography and computational quantum chemistry is a major methodology used to assess NLO-performances. As can be seen the non-centrosymmetric crystalline phases of (1) and (2) together with preliminary crystallographic results from derivative of the same chemical class shown in **Table 3** provide prospective reliable justification for further systematic research effort on their application-oriented aspects to photonics technologies as purely organic or metal-organics materials.

5. Conclusions

Let me conclude this study with the major point among others which could be drawn, as well. The crystals (1) and (2) are among the best cases of crystalline molecular templates of aliphatic amines allowing to model molecular packing depending on the space group type; thus, allowing us to assess the affect of the molecular structure and the mode of intermolecular interactions of crystal on the dynamic first hyperpolarizability in both the gas-phase and solution. Owing to the fact that the two major criteria of large first-order molecular hyperpolarizability data on crystals and their preferred crystallization into non-centrosymmetric space group type are required for generating innovative NLO-devices for application-oriented aspects of the photonics technologies, the crystallographically determined P1 and Pca2₁ space group types and large dynamics first-order molecular hyperpolarizability data together with their optical transparency within broad range of electromagnetic spectrum 190–1100 nm marked them as prospective templates for further application oriented research and development efforts for the discussed purposes.

Supplementary Materials: Experimental and theoretical optical spectroscopic and crystallographic data on crystals (**Figures S1–S9** and **Tables S1–S3**). CCDC 1567089 (1), and 1567095 (3) contain the supplementary crystallographic data on the crystals. They can be obtained free of charge via <http://www.ccdc.cam.ac.uk/conts/retrieving.html>, or from the Cambridge Crystallographic Data Centre, 12 Union Road, Cambridge CB2 1EZ, UK; fax: (+44) 1223-336-033; or e-mail: deposit@ccdc.cam.ac.uk.

Author Contributions: The author contributes to conceptualization; methodology; validation; formal analysis; investigation; resources; data curation; writing—original draft preparation; writing—review and editing; visualization. All authors have read and agreed to the published version of the manuscript.

Funding: This research received no external funding.

Institutional Review Board Statement: Not applicable.

Informed Consent Statement: Not applicable.

Data Availability Statement: Via request by the author.

Acknowledgments: The author is grateful to thank the Alexander von Humboldt Foundation for the Fellowships and the donation of single crystal X-ray diffractometer to the Department of Analytical Chemistry at the Faculty of Chemistry and Pharmacy at the Sofia University St. Kl. Ohridsk; the Deutsche Forschungsgemeinschaft; the Deutscher Akademischer Austausch Dienst for grant within priority program Stability Pact South-Eastern Europe for donation of UV-VIS-NIR Evolution 300 spectrometer, and the central instrumental laboratory clusters for mass spectrometry (currently, Centre of Mass Spectrometry) at Dortmund University.

Conflicts of Interest: The author declares no conflicts of interest.

References

1. Vermeulen, N.; Espinosa, D.; Ball, A.; Ballato, J.; Boucaud, P.; Boudebs, G.; Campos, C.; Dragic, P.; Gomes, A.; Huttunen, M.; Kinsey, N.; Mildren, R.; Neshev, D.; Padilha, L.; Pu, M.; Secondo, R.; Tokunaga, E.; Turchinovich, D.; Yan, J.; Yvind, K.; Dolgaleva, K.; Van Stryland, E. Post-2000 nonlinear optical materials and measurements: data tables and best practices. *J. Phys. Photonics* **2023**, *5*, 035001.
2. Annadhasan, M.; Basak, S.; Chandrasekhar, N.; Chandrasekar, R. Next-generation organic photonics: The emergence of flexible crystal optical waveguides. *Adv. Optical Mater.* **2020**, *8*, 2000959.
3. Ranjan, S.; Kumar, A.; Chandrasekar, R.; Takamizawa, S. Spatially controllable and mechanically switchable isomorphous organoferroelectric crystal optical waveguides and networks. *Nat. Commun.* **2024**, *15*, 74781.
4. Dalton, L.; Guenter, P.; Jazbinsek, M.; Kwon, O.; Sullivan, P. Organic Electro-Optics and Photonics. Cambridge University Press, Cambridge, 2015 [<https://doi.org/10.1017/CBO9781139043885.002>].
5. Zhang, Z.; Kim, J.; Khoury, R.; Saghaezhian, M.; Haber, L.; Plummer, E. Surface sum frequency generation spectroscopy on non-centrosymmetric crystal GaAs (001). *Surface Sci.* **2017**, *664*, 21–28.
6. Kleinman, D. Theory of second harmonic generation of light. *Phys. Rev.* **1962**, *128*, 1761–1775.
7. Franken, P.; Hill, A.; Peters, C.; Weinreich, G. Generation of optical harmonics. *Phys. Rev. Lett.* **1961**, *7*, 118–119.
8. Xiao, R.; Shao, D.; Gan, W.; Wang, H.; Han, H.; Sheng, Z.; Zhang, C.; Jiang, H.; Li, H. Classification of second harmonic generation effect in magnetically ordered materials. *npj Quantum Mater.* **2023**, *8*, 62.
9. Liu, X.; Bruch, A.; Lu, J.; Gong, Z.; Surya, J.; Zhang, L.; Wang, J.; Yan, J.; Tang, H. Beyond 100 THz-spanning ultraviolet frequency combs in a non-centrosymmetric crystalline waveguide. *Nat. Commun.* **2019**, *10*, 2971.
10. Zhao, M.; Ye, Z.; Suzuki, R.; Ye, Y.; Zhu, H.; Xiao, J.; Wang, Y.; Iwasa, Y.; Zhang, X. Atomically phase-matched second-harmonic generation in a 2D crystal. *Light: Sci. Appl.* **2016**, *5*, e16131.
11. Jha, K.; Dutta, S.; Munshi, P. Concomitance, reversibility, and switching ability of centrosymmetric and non-centrosymmetric crystal forms: Polymorphism in an organic nonlinear optical material. *Cryst. Growth Des.* **2018**, *18*, 1126–1135.

12. Zhang, X.; Li, X.; Cheng, Z.; Chen, A.; Wang, P.; Wang, X.; Lei, X.; Bian, Q.; Li, S.; Yuan, B.; Gao, J.; Li, F.; Pan, M.; Liu, F. Large-scale 2D heterostructures from hydrogen-bonded organic frameworks and graphene with distinct Dirac and flat bands. *Nat. Commun.* **2024**, *15*, 5934.
13. Fiebig, M.; Pavlov, V.; Pisarev, R. Second-harmonic generation as a tool for studying electronic and magnetic structures of crystals: review. *J. Opt. Soc. Am. B* **2005**, *22*, 96-118.
14. Raj, S.; Paiva, S.; Fritz, R.; Herrera, F.; Colón, Y. First-principles screening of metal-organic frameworks for entangled photon pair generation. *Mater. Quantum Technol.* **2024**, *4*, 015404.
15. Ivanova, B. Crystallographic and optical spectroscopic study of metal-organic 2D polymeric crystals of silver(I)- and zinc(II)-squarates. *Crystals* **2024**, *14*, 905.
16. Sagadevan, S. A simple theoretical approach to analyze the second harmonic generation of single crystals. *Optik* **2015**, *126*, 317-319.
17. Wang, L.; Rasskazov, I.; Carney, P. Clausius–Mossotti relation revisited: Media with electric and magnetic response. *Optics Commun.* **2023**, *549*, 129844.
18. Renugadevi, S.; Vijayaraghavan, G.; Mohaideen, H.; Balu, R. Optical and structural characterization of chemical components of *Calotropis procera* on semi-organic single crystal. *J. Mater. Sci.* **2024**, *35*, 1675.
19. Maschio, L.; Rérat, M.; Kirtman, B.; Dovesi, R. Calculation of the dynamic first electronic hyperpolarizability $\beta(-\omega_\sigma; \omega_1, \omega_2)$ of periodic systems. Theory, validation, and application to multi-layer MoS₂. *J. Chem. Phys.* **2015**, *143*, 244102.
20. Kaur, S.; Pandey, R.; Karna, S. Enhanced nonlinear optical response of graphene-based nanoflake van der Waals heterostructures. *RSC Adv.* **2021**, *11*, 5590-5600.
21. Rerat, M.; Maschio, L.; Kirtman, B.; Civalieri, B.; Dovesi, R. Computation of second harmonic generation for crystalline urea and KDP. An ab initio approach through the coupled perturbed Hartree-Fock/Kohn-Sham scheme. *J. Chem. Theory Comput.* **2016**, *12*, 107-113.
22. Bishop, D.; De Kee, D. The frequency dependence of nonlinear optical processes. *J. Chem. Phys.* **1996**, *104*, 9876-9887.
23. Bishop, D.; De Kee, D. The frequency dependence of hyperpolarizabilities for noncentrosymmetric molecules. *J. Chem. Phys.* **1996**, *105*, 8247-8249.
24. Xiao, R.; Shao, D.; Gan, W.; Wang, H.; Han, H.; Sheng, Z.; Zhang, C.; Jiang, H.; Li, H. Classification of second harmonic generation effect in magnetically ordered materials. *npj Quantum Mater.* **2023**, *8*, 62 [https://doi.org/10.1038/s41535-023-00594-3].
25. Ferrero, M.; Rérat, M.; Kirtman, B.; Dovesi, R. Calculation of first and second static hyperpolarizabilities of one- to three-dimensional periodic compounds. Implementation in the CRYSTAL code. *J. Chem. Phys.* **2008**, *129*, 244110.
26. Ivanova, B. Comment on “Comment on “Crystallographic and theoretical study of the atypical distorted octahedral geometry of the metal chromophore of zinc(II) bis((1R,2R)-1,2-diaminocyclohexane) dinitrate””. *J. Mol. Struct.* **2023**, *1287*, 135746.
27. Nalla, V.; Medishetty, R.; Wang, Y.; Bai, Z.; Sun, H.; Weid, J.; Vittal, J. Second harmonic generation from the ‘centrosymmetric’ Crystals. *IUCrJ* **2015**, *2*, 317-321.
28. Marsh, R. Centrosymmetric or noncentrosymmetric? *Acta Cryst.* **1986**, *B42*, 193-198.
29. Marsh, R. The centrosymmetric-noncentrosymmetric ambiguity: some more examples. *Acta Cryst.* **1994**, *A50*, 450-455.
30. Dougherty, J.; Kurtz, S. A second harmonic analyzer for the detection of non-centrosymmetry. *J. Appl. Cryst.* **1976**, *9*, 145-158.
31. Marsh, R. P1 or P-1? Or something else? *Acta Cryst.* **1999**, *B55*, 931-936.
32. Kaminskii, A. ; Bohaty, L. ; Becker, P. ; Eichler, H. ; Rhee, H. ; Maczka, M. ; Hanuza, J. Monoclinic ethylenediamine (+)-tartrate (NH₃CH₂CH₂NH₃)(+)-C₄H₄O₆ (EDT) – a new organic non-centrosymmetric crystal for Raman laser converters with large (3000 cm⁻¹) frequency shifts. *Laser Phys. Lett.* **2007**, *4*, 291-303.
33. Tomono, T. Potential of P1 organic crystal for compact SHG green laser. *Opt. Laser Technol.* **2015**, *68*, 2015, 220-224.
34. Osorio, M.; Valverde, C. Synthesis, crystal structure, spectroscopic and nonlinear optical properties of organic salt: A combined experimental and theoretical study. *J. Mol. Struct.* **2020**, *1210*, 128039.

35. Zhang, X.; Dong, H.; Hu, W. Organic semiconductor single crystals for electronics and photonics. *Adv. Mater.* **2018**, *30*, 1801048.
36. Shi, Y.; Zhuo, M.; Wang, X.; Liao, L. Two-dimensional organic semiconductor crystals for photonics applications. *ACS Appl. Nano Mater.* **2020**, *3*, 1080-1097.
37. Ma, Y.; Xu, C.; Mao, X.; Wu, Y.; Yang, J.; Xu, L.; Zhuo, M.; Lin, H.; Zhuo, S.; Wang, X. Oriented self-assembly of hierarchical branch organic crystals for asymmetric photonics. *J. Am. Chem. Soc.* **2023**, *145*, 9285-9291.
38. Fedorenko, E.; Mirochnik, A.; Gerasimenko, A.; Lyubykh, N.; Beloliptsev, A.; Mayor, A.; Egorov, A.; Kostyukov, A.; Burtsev, I.; Nguyen, T.; Shibaeva, A.; Markova, A.; Kuzmin, M. Molecular design of substituted boron difluoride curcuminoids: Tuning luminescence and nonlinear optical properties. *J. Photochem. Photobiol. A* **2025**, *460*, 116110.
39. Pradeep, V.; Chosenyah, M.; Mamonov, E.; Chandrasekar, R. Crystal photonics foundry: geometrical shaping of molecular single crystals into next generation optical cavities. *Nanoscale* **2023**, *15*, 12220.
40. Qiu, L.; Lv, Q.; Wang, X. Low-dimensional organic semiconductor crystals for advanced photonics. *Moore More* **2024**, *1*, 10.
41. Bose, A.; Banerjee, R.; Narayan, A. Pressure-induced magnetic and topological transitions in non-centrosymmetric MnIn₂Te₄. *J. Phys.* **2024**, *36*, 505807.
42. Sivaranjani, R.; Suvitha, A.; Garg, M.; Arumanayagam, T. Exploring linear and nonlinear optical behaviour of morpholine p-nitrophenol crystal: Computational and experimental analysis. *Chem. Phys. Impact* **2023**, *7*, 100363.
43. Shen, C.; Sun, D.; Dang, Y.; Wu, K.; Xu, T.; Hou, R.; Chen, H.; Wang, J.; Wang, D. (C₄H₁₀NO)PbX₃ (X = Cl, Br): Design of two lead halide perovskite crystals with moderate nonlinear optical properties. *Inorg. Chem.* **2022**, *61*, 42, 16936-16943.
44. Sudhakar, G.; Babu, D. Synthesis and characterization of piperazine nitrate monochloride semi-organic single crystal for NLO applications. *Discov. Appl. Sci.* **2024**, *6*, 645.
45. Chen, J.; Wu, H.; Xu, M.; Wang, M.; Chen, Q.; Li, B.; Hu, C.; Du, K. Halide-driven polarity tuning and optimized SHG-bandgap balance in (C₄H₁₁N₂)ZnX₃ (X = Cl, Br, I). *Inorg. Chem. Front.* **2024**, *11*, 5587-5597.
46. Steffy, A.; Dhas, D.; Joe, I.; Balachandran, S. Computational study on piperazine-1,4-dium acetate using dft investigations: Structural aspects, topological and nonlinear optical properties. *Cryst. Res. Technol.* **2024**, *59*, 2300151.
47. Sudhakar, G.; Babu, D. Growth and characterization of piperazine oxalic acid monochloride semiorganic NLO single crystals. *Opt. Mater.* **2024**, *150*, 115123.
48. Patent: UNIVERSITY OF FLORIDA RESEARCH FOUNDATION - WO2020/163823, 2020, A2.
49. Patent: JANSSEN PHARMACEUTICA - WO2022/159976, 2022, A1.
50. Li, S.; Zhao, J.; Zhang, Z.; Zhang, J.; Yang, W. Synthesis and characterization of aliphatic thermoplastic poly(ether urethane) elastomers through a non-isocyanate route. *Polymer* **2015**, *57*, 164-172.
51. Patent: HIBERNIA-Chem.- BE621259, 1962, A [Chem.Abstr., 1963, vol. 59, #8616h].
52. Patent: HIBERNIA-US3352913, 1961, A [Chem.Abstr., 1968, vol. 68, #12553z].
53. Zagidullin, R. Aminomethylation of N-(β-amonoethyl)piperazine and its derivatives. *J. Gen. Chem. USSR* **1991**, *61*, 225-230.
54. Ivanova, B.; Spitteller, M. CCDC 1583979: Experimental Crystal Structure Determination, 2013 [DOI: 10.5517/ccdc.csd.cc1q5838].
55. Ivanova, B.; Spitteller, M. Heptachlorepoxydes: theoretical versus experimental study of the embedded samples in the matrixes of organic crystals. *J. Incl. Phenom. Macrocycl. Chem.* **2013**, *76*, 415 [DOI: 10.1007/s10847-012-0213-x].
56. Ivanova, B.; Spitteller, M. CCDC 881820: Experimental Crystal Structure Determination, 2013 [DOI: 10.5517/ccylltx].
57. Ivanova, B.; Spitteller, M. CCDC 775457: Experimental Crystal Structure Determination, 2013 [DOI: 10.5517/ccv0xrh].
58. Ivanova, B.; Spitteller, M. CCDC 881821: Experimental Crystal Structure Determination, 2013 [DOI: 10.5517/ccyllvy].

59. Ivanova, B.; Spiteller, M. Chapter: Experimental mass spectrometric and theoretical treatment of the effect of protonation on the 3D molecular and electronic structures of low molecular weight organics and metal-organics of silver(I) ion; In *Protonation: Properties, Applications and Effects*, A. Germogen (Ed.). NOVA Science Publishers, New York, 2019, pp.1–141.
60. Ivanova, B.; Spiteller, M. CCDC 1584573: Experimental Crystal Structure Determination, 2019 [DOI: 10.5517/ccdc.csd.cc1q5w81].
61. Sheldrick, G. A short history of SHELX. *Acta Cryst.* **2008**, A64, 112-122.
62. Sheldrick, G. Experimental phasing with SHELXC/D/E: combining chain tracing with density modification. *Acta Cryst.* **2010**, D 66, 479-485.
63. Sheldrick, G. Phase annealing in SHELX-90: direct methods for larger structures. *Acta Cryst.* **1990**, A 46, 467-473.
64. Bourhis, L.; Dolomanov, O.; Gildea, R.; Howard, J.; Puschmann, H. The anatomy of a comprehensive constrained, restrained refinement program for the modern computing environment – Olex2 dissected. *Acta Cryst.* **2015**, A71, 59-75.
65. Dolomanov, O.; Bourhis, L.; Gildea, R.; Howard, J.; Puschmann, H. OLEX2: a complete structure solution, refinement and analysis program. *J. Appl. Cryst.* **2009**, 42, 339-341.
66. Spek, A. Single-crystal structure validation with the program PLATON. *J. Appl. Cryst.* **2003**, 36, 7-13.
67. Farrugia, L. WinGX and ORTEP for Windows: An Update. *J. Appl. Cryst.* **2012**, 45, 849 [http://www.chem.gla.ac.uk/~louis/software/wingx/].
68. Dunitz, J.; Schomaker, V.; Trueblood, K. Interpretation of atomic displacement parameters from diffraction studies of crystals. *J. Phys. Chem.* **1988**, 92, 856.
69. Dunitz, J.; Maverick, E.; Trueblood, K. Atomic motions in molecular crystals from diffraction measurements. *Angew. Chem., Int Ed.* **1988**, 27, 880.
70. Frisch, M.; Trucks, G.; Schlegel, H. et al. (2009) (1998), Gaussian 09, 98. Gaussian Inc, Pittsburgh [www.gaussian.com]
71. Dalton2011 Program Package. [https://www.daltonprogram.org/download.html]
72. Gordon, M.; Schmidt, M. Advances in electronic structure theory: GAMESS a decade later. In: Dykstra C, Frenking G, Kim K, Scuseria G (eds) *Theory and Applications of Computational Chemistry: the first forty years*. Elsevier, Amsterdam, 2005, pp 1167-1189.
73. GausView03 Program Package [www.gaussian.com/g_prod/gv5.htm].
74. Zhao, Z.; Truhlar, D. Density functionals with broad applicability in chemistry. *Accs. Chem. Res.* **2008**, 41, 157-167.
75. Zhao, Y.; Truhlar, D. The M06 suite of density functionals for main group thermochemistry, thermochemical kinetics, noncovalent interactions, excited states, and transition elements: two new functionals and systematic testing of four M06-class functionals and 12 other functionals. *Theor. Chem. Acc.* **2008**, 120, 215-241.
76. Hay, P.; Wadt, W. Ab initio effective core potentials for molecular calculations. Potentials for K to Au including the outermost core orbitals. *J. Chem. Phys.* **1985**, 82, 299.
77. Burkert, U.; Allinger, N. *Molecular mechanics in ACS Monograph 177*. American Chemical Society, Washington DC, 1982, pp 1-339.
78. Allinger, L. Conformational analysis. 130. MM2. A hydrocarbon force field utilizing V1 and V2 torsional terms. *J. Am. Chem. Soc.* **1977**, 99, 8127-8134.
79. Casida, M. Time-dependent density functional response theory for molecules. in *Recent Advances in Density Functional Methods 155–192*, World Scientific, 1995.
80. Van Gisbergen, S.; Snijders, J.; Baerends, E. Implementation of time-dependent density functional response equations. *Comput. Phys. Comm.* **1999**, 118, 119-138.
81. Hirata, S.; Head-Gordon, M. Time-dependent density functional theory within the Tamm–Dancoff approximation. *Chem. Phys. Lett.* **1999**, 314, 291-299.
82. Mostafa, A.; Bazzi, H. Charge-transfer complexes of 1-(2-aminoethyl) piperazine with σ - and π -acceptor. *J. Mol. Struct.* **2010**, 983, 153-161.
83. Patent: UBE INDUSTRIES - US2012/302782, 2012, A1.

84. Chankeshwara, S.; Chakraborti, A. Indium(III) halides as new and highly efficient catalysts for N-tert-butoxy-carbonylation of amines. *Synthesis* **2006**, *16*, 2784-2788.
85. Ferrero, M.; Rérat, M.; Orlando, R.; Dovesi, R. Coupled perturbed Hartree-Fock for periodic systems: The role of symmetry and related computational aspects. *J. Chem. Phys.* **2008**, *128*, 014110.
86. Huber, H.; Sommer-Jørgensen, M.; Gubler, M.; Goedecker, S. Targeting high symmetry in structure predictions by biasing the potential energy surface. *Phys. Rev. Res.* **2023**, *5*, 013189.
87. Marsh, R. Space group P1: an update. *Acta Cryst.* **2005**, *B61*, 359.
88. Steed, K.; Steed, J. Packing problems: High Z' crystal structures and their Relationship to cocrystals, inclusion compounds, and polymorphism. *Chem. Rev.* **2015**, *115*, 2895-2933.
89. Mohanapriya, E.; Janczak, J.; Al-Mohaimed, A.; Al-onazi, W.; Kanagathara, N.; Marchewka, M. Structure, vibrational characterization and SHG of the recrystallization product of L-phenylalanine from aqueous HCl solution. *J. Mol. Struct.* **2025**, *1319*, 139532.
90. Gonçalves, M.; Silva, M. Experimental and calculated second harmonic generation of a guanidinium salt in the solid state. *Solid State Commun.* **2020**, *314-315*, 113853.
91. [91] T. Hrivnák, M. Medved, W. Bartkowiak, R. Zalesny, Hyperpolarizabilities of push-pull chromophores in solution: Interplay between electronic and vibrational contributions. *Molecules* **2022**, *27*, 8738.
92. Potla, K.; Nuthalapati, P.; Osorio, J.; Valverde, C.; Vankayalapati, S.; Adimule, S.; Armakovic, S.; Armakovic, S.; Mary, Y. Multifaceted study of a Y-shaped pyrimidine compound: Assessing structural properties, docking interactions, and third-order nonlinear optics. *ACS Omega* **2024**, *9*, 7424-7438.
93. Kim, K.; Li, Y.; Ok, K. Hafnium-based chiral 2D organic-inorganic hybrid metal halides: Engineering polarity and nonlinear optical properties via *para*-substituent effects. *J. Am. Chem. Soc.* **2025** [<https://doi.org/10.1021/jacs.4c16985>].
94. Zhao, Y.; Li, M.; Zhao, X.; Yuan, K.; Chen, W. A lithium cycloparaphenylene as an emerging second-order non-linear optical molecular switch. *Cell Rep. Phys. Sci.* **2023**, *4*, 101653.
95. Simsek, M.; Tamer, O.; Dege, N.; Avci, D.; Atalaz, Y. Investigation on the effect of complex formation on prominent high static/dynamic first and second hyperpolarizability of Co(II) complex including 4-chloro-pyridine-2-carboxylic acid. *Mater. Sci. Semicond. Proc.* **2025**, *188*, 109179.
96. Bhoday, H.; Knotts, N.; Glaser, R. Perfect polar alignment of parallel beloamphiphile layers: Improved structural design bias realized in ferroelectric crystals of the novel methoxyphenyl series of acetophenone azines. *Chem. Eur. J.* **2024**, *30*, e202400182.
97. Lin, J.; Zhou, J.; Wang, Z.; Li, L.; Li, M.; Xu, J.; Wu, S.; Naumov, P.; Gong, J. Low-temperature flexibility of chiral organic crystals with highly efficient second-harmonic generation. *Angew. Chem. Int. Ed.* **2024**, e202416856.
98. Araújo, R.; Abegão, L.; Ribeiro, C.; Rodrigues Jr, J.; Valle, M.; Alencar, M. Unveiling nonlinear optical behavior in benzophenone and benzophenone hydrazone derivatives. *Appl. Phys. B* **2024**, *130*, 124.
99. Swamynayaka, S.; Venkatesha, K.; Harish, K.; Revanna, B.; Venkatesh, C.; Madegowda, M.; Hegde, T. Third-order nonlinear response of a novel organic acetohydrazide derivative: Experimental and theoretical approach, *Opt. Mater.* **2023**, *139*, 113826.
100. Ziadi, K.; Messaoudi, A. A theoretical investigation of second-order nonlinear optical properties in push-pull π -conjugated compounds, including phenoxazine-based systems. *Comput. Theor. Chem.* **2025**, *1244*, 115049.
101. Araújo, R.; Abegão, L.; Ribeiro, C.; Rodrigues Jr, J.; Valle, M.; Alencar, M. Unveiling nonlinear optical behavior in benzophenone and benzophenone hydrazone derivatives. *Appl. Phys.* **2024**, *B 130*, 124.
102. Pachaiyappan, S.; Kumaresan, P.; Kamatchi, T.; Nithiyantham, S.; Logeswari, J.; Kumar, K. Molecular electrostatic potential (MEP), thermodynamic properties and spectral analysis of methyl orange doped L-lysine sulfate (MLLS) semi organic crystals. *Vietnam J. Chem.* **2024**, *62*, 670-679.
103. Ivanova, B.; Spiteller, M. Matrix-assisted laser desorption/ionization mass spectrometric analysis of herbicides in dication-containing organic crystals. *Anal. Meth.* **2012**, *4*, 4360 [DOI: 10.1039/C2AY26072G].
104. Ivanova, B.; Spiteller, M. CCDC 760142: Experimental Crystal Structure Determination, 2012, [DOI: 10.5517/ccthzqz].

105. Ivanova, B.; Spiteller, M. CCDC 882498: Experimental Crystal Structure Determination, 2012, [DOI: 10.5517/ccym9pj].
106. Ivanova, B.; Spiteller, M. Solid-state UV-MALDI mass spectrometric quantitation of fluroxypyr and triclopyr in soil. *Environm. Geochem. Health* **2015**, *37*, 557.
107. Ivanova, B.; Spiteller, M. CCDC 770390: Experimental Crystal Structure Determination, 2012, [DOI: 10.5517/ccdc.csd.cctvn9l].
108. Ivanova, B.; Spiteller, M. Chapter: Mass Spectrometric Experimental and Theoretical Quantification of Reaction Kinetics, Thermodynamics and Diffusion of Piperazine Heterocyclics in Solution, In: *Advances in Chemistry Research*, J. Taylor (Ed.), NOVA Science Publishers Inc. N.Y., 2019, pp.1-82.
109. Ivanova, B.; Spiteller, M. CCDC 775456: Experimental Crystal Structure Determination, 2016, [DOI: 10.5517/ccdc.csd.ccv0xqg].
110. Lamshoft, M.; Storp, J.; Ivanova, B.; Spiteller, M. Gas-phase CT-stabilized Ag(I) and Zn(II) metal–organic complexes – Experimental versus theoretical study. *Polyhedron* **2011**, *30*, 2564.
111. Lamshoft, M.; Storp, I.; Ivanova, B.; Spiteller, M. CCDC 832306: Experimental Crystal Structure Determination, 2011, [DOI: 10.5517/ccwy2lg].
112. Ivanova, B.; Spiteller, M. CCDC 792094: Experimental Crystal Structure Determination, 2013, [DOI: 10.5517/ccvl7f2].
113. Ivanova, B.; Spiteller, M. Factors stabilizing the gas-phase ionic species of crystals of organic salts – Experimental and theoretical study. *J. Mol. Struct.* **2013**, *1036*, 226, [DOI: 10.1016/j.molstruc.2012.11.018].
114. Vivas, M.; Barboza, C.; Germino, J.; Fonseca, R.; Silva, D.; Vazquez, P.; Atvars, T.; Mendonc, C.; De Boni, L. Molecular structure-optical property relationship of salicylidene derivatives: A study on the first-order hyperpolarizability. *J. Phys. Chem. A* **2021**, *125*, 99-105.

Disclaimer/Publisher's Note: The statements, opinions and data contained in all publications are solely those of the individual author(s) and contributor(s) and not of MDPI and/or the editor(s). MDPI and/or the editor(s) disclaim responsibility for any injury to people or property resulting from any ideas, methods, instructions or products referred to in the content.